A Study on the Preparation and Performance Optimization of Alkali-Activated Fly Ash-Based Aerogel-Modified Foam Concrete

Peng Liu , Wei Wu , Yanfeng Gong *

Posted Date: 24 November 2025

doi: 10.20944/preprints202511.1691.v1

Keywords: ultra-low energy consumption buildings; FA; high-performance AAFC; SiO_2 aerogel; waterproofing

 doi:10.20944/preprints202511.1691.v1

Article

A Study on the Preparation and Performance Optimization of Alkali-Activated Fly Ash-Based Aerogel-Modified Foam Concrete

Peng Liu [1,2], Wei Wu [2] and Yanfeng Gong [2,*]

[1] Jiangsu Vocational Institute of Architectural Technology, Jiangsu Collaborative Innovation Center for Building Energy Saving and Construct Technology, Xuzhou, Jiangsu 221000, China

[2] College of Civil Engineering, Nanjing Tech University, Nanjing, Jiangsu 210000, China

* Correspondence: catherine19890107@163.com

Abstract

To address the energy-saving requirements of ultra-low energy consumption buildings in hot summer and cold winter regions, high-performance foam concrete(FC)was developed using fly ash(FA) as the sole silico-aluminous raw material using alkali-activation technology. A mix proportion calculation model was established based on the volume method to accomplish the preliminary design of the material system, and orthogonal tests were employed to achieve the synergistic enhancement of thermal, mechanical, and other relevant properties. Innovatively, the introduction of the 2.5 wt% SiO_2 aerogel reduced the thermal conductivity to 0.1107 W/(m·K). To mitigate the high water absorption of FC, internal mixing with a sodium methyl silicate solution (at a concentration of 8%) controlled the mass water absorption by 3.87%. Test results confirmed that the optimized FC exhibited a dry density of 576.34 kg/m^3, compressive and flexural strengths of 5.83 MPa and 1.41 MPa respectively, a dry shrinkage rate of only 0.614 mm/m, and strength and mass loss rates below 10.5% and 1.8% after freeze-thaw cycling. This material integrates ultralow thermal conductivity, excellent hydrophobicity, and structural stability, thereby providing a novel solution for the envelope structures of low-energy consumption buildings.

Keywords: ultra-low energy consumption buildings; FA; high-performance AAFC; SiO_2 aerogel; waterproofing

1. Introduction

The global environmental crisis is intensifying, and projections indicate that the building sector in China will account for over 40% of total societal energy consumption by 2050[1]. The development of energy-efficient materials, such as FC, is therefore crucial for the sustainable development of the construction industry. FC offer advantages such as thermal insulation, fire resistance, and low cost. However, a significant paradox exists: conventional FC relies on Ordinary Portland Cement (OPC), a binder with a highly energy-intensive production process that contributes to approximately 8% of the global carbon emissions [2]. In contrast, Alkali-Activated Materials (AAMs), which can reduce associated carbon emissions by over 80% [3], present a sustainable alternative and are widely recognized as "green cement."

The properties of AAFC are significantly influenced by the raw material composition, activator parameters, and production methods. Waste utilization strategies significantly enhance specific properties: FA with clinoptilolite improves thermal and frost resistance [4,5], pinecone powder increases the 91-day strength by 256.6% [6], recycled brick powder with Na_2O reduces thermal conductivity to 0.1067–0.1121 W/(m·K) [7,8], and waste glass enhances mechanical and corrosion resistance[9]. Process optimization through red mud addition and mechanical activation improves the pore structure and strength [10,11], while advanced composites containing hollow glass beads,

 doi:10.20944/preprints202511.1691.v1

rice husk, silica fume, and FA demonstrate synergistic thermal-mechanical performance enhancement [12–15].

Lightweight design strategies are implemented through the incorporation of Expanded Polystyrene (EPS) beads[16], waste polyurethane (PUR) [17], and lightweight aggregates [18], with densities of ≤800 kg/m^3 and thermal conductivity as low as 0.07 W/(m·K) being achieved. Foaming techniques, including chemical (H_2O_2 and zinc/aluminum metal powders) and physical methods (Sodium Dodecyl Sulfate(SDS)), allow tailored pore structures. The H_2O_2/SDS combination enables the production of materials with either ultra-low thermal conductivity (0.072W/(m·K)) or high compressive strength (19.6MPa)[19–21], demonstrating flexibility in property design through processing optimization.

The pore characteristics critically govern the thermal and mechanical properties of AAFC. Jaya et al.[22]identified that the activator composition primarily controls the compressive strength (0.4–6MPa), whereas the precursor/activator ratio dictates the thermal conductivity (0.11–0.30 W/(m·K)). The synergistic use of H_2O_2 and Tween 80 enabled porosity control within 36–86%. A more than two-fold increase in the 28-day strength was achieved by Su et al.[23] by optimizing the activator modulus (SiO_2/Na_2O=1.2–1.8) under high-humidity curing conditions (RH≥90%). A key research challenge is to balance low thermal conductivity with high strength. Huan et al.[24]developed a hierarchically porous material with 93.8% porosity and 0.040 W/(m·K) thermal conductivity, albeit at low strength (0.27 MPa). In contrast, Berkouche et al.[25]balanced both properties (0.13 W/(m·K), 4.26 MPa) using rice husk ash (RHA) and glass powder (GP). RHA enhanced the strength through geopolymerization, whereas GP refined the pore structure as an inert filler. The microstructural analysis confirmed that the performance stems from the synergy between the gel phases (C-A-S-H/N-A-S-H) and pore distribution.

Nanomaterials provide a superior approach for tailoring material properties. Rong et al.[26]demonstrated that combining 12% aerogel with 75% foam reduces thermal conductivity to 0.18 W/(m·K), while adding 1% polypropylene fibers increases compressive strength to 23.7 MPa. Similarly, Pan et al.[27]found that silica aerogel decreases the thermal conductivity by 24% (to 0.0886 W/(m·K)) through multi-scale porosity, and Ji et al.[28] reported that 0.4% CMC enhances the pore structure, improving the strength by 44.7% and pore sphericity.

While existing research often prioritizes the extreme optimization of one or a few properties, such as achieving ultralow thermal conductivity, a more holistic approach was adopted in this study. Using FA-based AAFC as the matrix, this work is designed around the multi-performance requirements of envelope materials for ultra-low energy consumption buildings. A comprehensive set of seven key indicators was established, including thermal conductivity, mechanical strength, fire resistance, and freeze-thaw durability. Notably, a critical focus is placed on enhancing waterproofing performance, effectively addressing the long-standing issue of high water absorption in FC. Specifically, SiO_2 aerogel, a super thermal insulation material, was incorporated to enhance the thermal performance of AAFC. Resolve the conflict between the mechanical and thermal properties of conventional FC. Ultimately, all parameters met the requirements of the performance index system. A synergistic enhancement in the range of key material properties was achieved.

2. Construction of Target Performance Index System for AAFC

2.1. Determination of Target Performance Indicators and Parameters

To address the energy efficiency requirements of ultra-low energy consumption buildings in hot-summer and cold-winter regions, a high-performance AAFC has been developed with the objective of achieving self-insulation through 300 mm-thick exterior walls, satisfying mechanical standards for non-load-bearing walls, demonstrating excellent water resistance, and conforming to specifications for dry density, fire resistance, and frost resistance.

 doi:10.20944/preprints202511.1691.v1

(1) Dry Density and Mechanical Properties

The dry density was optimized by balancing the sound insulation and the mechanical requirements. For non-load-bearing exterior walls, mechanical targets–compressive strength, flexural strength, and drying shrinkage–were defined according to relevant standards[29–31].

(2) Thermal Performance

The thermal performance was characterized by two key parameters: wall thermal transmittance and thermal conductivity of the AAFC. To fulfill the self-insulation criteria for ultra-low energy buildings in hot-summer and cold-winter regions, the thermal transmittance was limited to ≤0.4 W/(m²·K) [32–34]. The exterior wall thickness is set to 300 mm. The thermal conductivity of the AAFC was then calculated in compliance with the relevant design codes, as follows[35]:

$$K = 1/\left(1/h_1 + 1/h_2 + \delta/\lambda\right) \quad (1)$$

In the equation, K(0.4 W/(m◎K)) is the wall thermal transmittance; h_1 and h_2 are the interior and exterior surface heat transfer coefficients, taken as 8.7 and 23 W/(m²·K) respectively, with the latter representing the most severe condition; δ is the wall thickness (0.3 m); λ is the thermal conductivity of the AAFC(W/(m·K)); and a thermal conductivity correction factor (α) of 1.05 was incorporated. Thus, the corresponding thermal conductivity of AAFC should not exceed 0.1216 W/(m·K).

(3) Fire Resistance and Water Resistance

The AAFC material exhibits Class A fire resistance as an inorganic noncombustible material,thus meeting these requirements.

To address the inherent drawback of high water absorption in FC, mass water absorption was adopted as a key performance indicator. The influence of moisture content (varied from 0% to 55% at 5% intervals) on thermal conductivity was investigated using the weight method. A well-fitted correlation (R^2=0.97669) was established between the thermal conductivity and water absorption, demonstrating a significant dependence of thermal performance on moisture content.

$$\lambda = 0.2016 + 0.00853x - 0.0001x^2 \quad (2)$$

where λ is the thermal conductivity of the AAFC(W/(m·K)), x is the mass water absorption (%); the results are shown in the figure below:

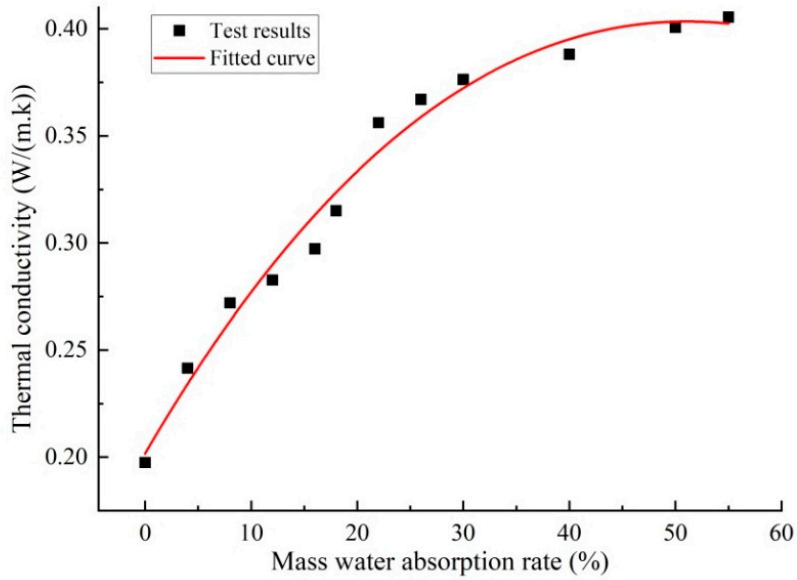

Figure 1. Fitting curve of thermal conductivity with mass water absorption rate.

 doi:10.20944/preprints202511.1691.v1

The thermal conductivity exhibited a significant dependence on mass water absorption, increasing by 105.31% from 0.1975 W/(m·K) in the dry state to 0.4055 W/(m·K) at 55% moisture content (Figure 1). A near-linear rapid rise occurred within 0–10% absorption, where the conductivity exceeded the target value by 37.35%. Given that the existing standards are inadequate for practical requirements [29], the mass water absorption is targeted at ≤5% based on a comprehensive analysis.

(5) Frost Resistance

According to national standards, the frost resistance for the hot summer and cold winter (non-central-heating) region is set as F25 [36], with the strength and mass loss rates serving as the secondary indicators.

2.2. Target Performance Indexes of AAFC

According to the requirements in Section 2.1, the target performance indices established in this study and the corresponding values are presented in the Table 1 below.

Table 1. Target performance indexes.

First-level Indicator Type	Second-level Indicator Name	Target Value
Bulk Density	Dry Density ϱ	A06 (⩽650 kg/m³)
Thermal Performance	Thermal Transmittance K	Wall Thickness 300mm，⩽0.4 W/m²·K
	Thermal Conductivity λ	⩽0.1216W/(m·K)
Fire Resistance	Combustion Performance Rating F_{RL}	Class A (Non-Combustible Material)
Water Resistance	Mass Water Absorption Wr	⩽5%
Mechanical Properties	Compressive Strength f	⩾5 MPa
	Flexural Strength R_f	⩾1.0 MPa
	Drying Shrinkage ε	⩽1 mm/m
Frost Resistance(F25)	Strength Loss Rate F_c	⩽25%
	Mass Loss Rate M_m	⩽5%

3. Mix Proportion Design Method for AAFC

3.1. Basic Principles

A mix proportion design method for AAFC was developed based on the volume method, which operates on the principle that the volume of the fresh slurry equals the sum of the volumes of all solid components and the entrapped air. In this approach, the target performance values are first established, followed by theoretical calculations of raw material dosages and experimental refinement. The dry density was selected as the primary design target because of its ease of control.

3.2. Design Steps and Calculation Methods for Mix Proportion

Based on the above principles, the mix proportion design steps for the AAFC are as follows:

(1) The mass of each precursor component and other curable materials was determined according to the target dry density of the AAFC.

(2) Determine the water-to-binder ratio, activator dosage, and additional water amount, based on the precursor dosage.

 doi:10.20944/preprints202511.1691.v1

(3) The volume of each constituent material in the slurry was calculated to determine the foam volume.
(4) The foam mass was determined using the calculated foam volume and foam density.
(5) The required foaming agent mass was calculated based on its dilution ratio and foam mass.

The mix proportion design relationship for the precursor (including silico-aluminate raw materials)–activator–physical foaming system is:

$$\rho_d = \left(m_{pre} + m_{act} + \sum_{i=1}^{n} m_i \right) \times S_a \tag{3}$$

where ρ_d denotes the design dry density of AAFC (kg/m³); m_{pre} represents the mass of precursor materials in 1 m³ of AAFC (kg); m_{act} is the mass of the curable portion of the alkali activator in 1 m³ of AAFC (kg); m_i denotes the mass of each additional curable raw material in 1 m³ of AAFC (kg); S_a is the mass coefficient determined by the total dry material mass of each component and the total non-evaporable matter in the finished product after curing of AAFC, with a range of 1.0 to 1.3, determined experimentally.

In the preparation of 1 m³ AAFC slurry, the sum of the volumes of silico-aluminate-containing precursor materials, activator, water required except for diluting the foaming agent, and other curable raw materials is denoted as V_1, which is calculated using Eq.4; The portion where the slurry volume is less than 1 m³ is considered to be filled by foam, and the foam volume V_2 can be calculated using Eq.5.

$$V_1 = \frac{m_{pre}}{\rho_{pre}} + \frac{m_{act}}{\rho_{act}} + \frac{m_w}{\rho_w} + \sum_{i=1}^{n} m_i \Big/ \sum_{i=1}^{n} \rho_i \tag{4}$$

where V_1 denotes the sum of the volumes of precursor materials, activator, water required except for diluting the foaming agent, and other curable raw materials (m³); m_w represents the mass of water required except for diluting the foaming agent (kg); ρ_{pre} is the density of the precursor materials (kg/m³); ρ_{act} is the density of the prepared activator (kg/m³); ρ_w is the density of water (kg/m³), with a value of 1000 kg/m³; ρ_i denotes the respective densities of other curable raw materials in the AAFC (kg/m³).

$$V_2 = k\,(1 - V_1) \tag{5}$$

where V_2 denotes the foam content in 1 m³ of AAFC (m³/m³); k is the surplus coefficient, which should be determined according to the type and quality of the foaming agent, foam preparation time, etc., for foaming agents with good stability; the value range is 1.1 to 1.4; and the specific value is determined through experimental and theoretical analysis.

The dosage of the foaming agent m_f in 1 m³ of AAFC can be calculated using Eq.6 and 7:

$$m_p = V_2 \times \rho_{foam} \tag{6}$$

where m_p denotes the mass of foam in 1 m³ of AAFC (kg) and ρ_{foam} denotes the mass of foam in 1 m³ of FC (kg).

$$m_f = m_p \div (\beta + 1) \tag{7}$$

where m_f denotes the dosage of foaming agent in 1 m³ of AAFC (kg) and β represents the dilution multiple of the foaming agent, which can be determined through experiments.

3.3. Test Raw Materials and

(1) FA and activators

FA from Xuzhou China Resources Power Co., Ltd., was used as the primary raw material. A binary composite activator was prepared by mixing water glass (modulus=3.3, Baume degree =38.5°Be') from Yourui Refractory Materials Co., Ltd. with sodium hydroxide (NaOH, ≥99% purity, IS-I grade) supplied by Shandong Binzhou Chemical Group Co., Ltd.

 doi:10.20944/preprints202511.1691.v1

(2) Foaming Agents

The HTQ-1 composite polymer foaming agent was supplied by Henan Huatai New Material Technology Co. Ltd. Its performance was tested in accordance with the national standards [37] under a foaming pressure of 0.5 MPa. The foaming performance parameters are listed in Table 2.

Table 2. Performance parameters of foaming agent.

Project	Foaming Agent Multiple n	1-hour sedimentation distance (mm)		Sedimentation distance (cm/h)	
		First-class product	Qualified Product	First-class product	Qualified Product
Indicator	15~30	≤50	≤70	≤70	≤80
Test Results	28	41.1		59.6	

(3) Lightweight Aggregate—Vitrified Microspheres

Lightweight aggregates can reduce density while enhancing mechanical properties. Vitrified microspheres (Figure 2(a)) from Hebei Yixin Energy Conservation and Thermal Insulation Building Materials Co., Ltd., were used, and their properties are listed in Table 3.

Table 3. Performance parameters of vitrified microbeads.

Particle size(mm)	Bulk density (kg/m$^{3)}$	Cylinder pressure strength (MPa)	Thermal conductivity (W/(m·K))	Water absorption rate(%)	Floating rate(%)	Surface vitrification closed-cell rate (%)	Linear shrinkage rate (%)
1~3	116	0.52	0.049	30	≥80	≥80	0.29

(4) Basalt Fiber

The fibers enhanced the tensile strength of FC. Basalt fibers (Figure 2(b)) from Changsha Ningxiang Building Materials Co., Ltd. were used, and their properties are listed in Table 4.

Table 4. Performance parameters of basalt fibers.

Fiber length mm	Relative density g/cm^3	Diameter μm	Elastic modulus GPa	Tensile strength MPa	Ultimate elongation %
6	2.65	17	7.6	1050	3

(5) Foam stabilizers.

Hydroxypropyl methylcellulose ether (HPMC) was used as the foam stabilizer. A white powder (Figure 2(c)) with a molecular weight of 86,000 and a viscosity of 200,000 effectively thickens the foam film and reduces defoaming or bubble merging.

(6) Calcium Hydroxide

Low-calcium ash was used as the FA. Calcium hydroxide was added to enhance the mechanical properties of the AAFC. Calcium hydroxide powder (Figure 2(d)) was supplied by Nanjing Baore Chemical Co. Ltd.

(7) Waterproofing agents.

The internally admixed waterproofing agent sodium methyl silicate solution, as shown in Figure 2(e), was produced by Shanxi Jing Chen Building Materials Co., Ltd.

 doi:10.20944/preprints202511.1691.v1

Figure 2. Raw materials, (a) vitrified microbeads, (b) basalt fiber, (c) HPMC, (d) calcium hydroxide, (e) sodium methylsilicate solution.

(8) SiO_2 Aerogel

The SiO_2 aerogel was supplied by Shenzhen Zhongning Technology Co., Ltd., and its performance parameters are summarized in Table 5 below.

Table 5. Performance parameters of silica aerogel powder.

Particle size μm	Bulk density kg/m³	Pore diamete rnm	Porosity %	Specific surface area m²/g	Thermal conductivity W/(m·K)	Surface properties
15~50	40~60	20~50	＞90	500~800	＜0.013	Hydrophobic

(a) SiO_2 Aerogel Powder

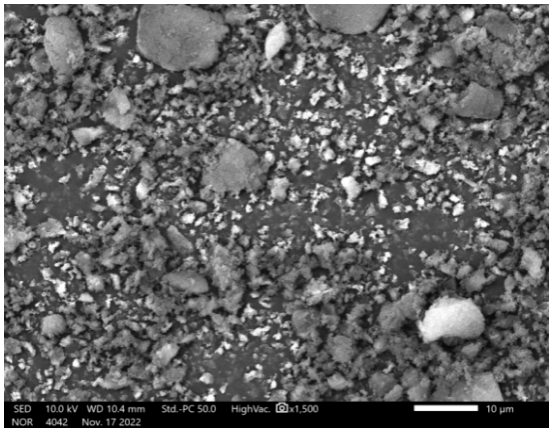

(b) Microstructure of SiO_2 Aerogel

 doi:10.20944/preprints202511.1691.v1

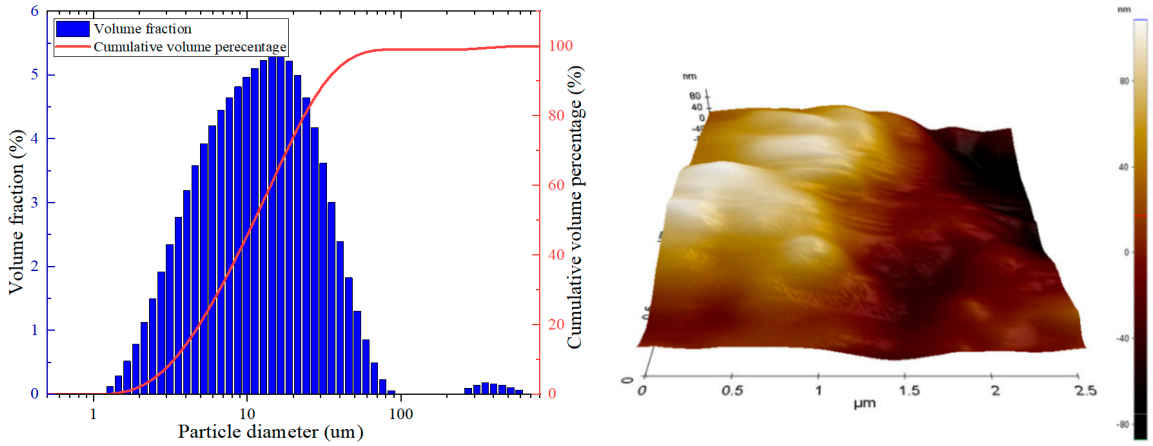

(c) Particle Size Distribution of SiO_2 Aerogel (d) Surface Roughness

Figure 3. Silica aerogel powder and its microscopic characteristics.

The SiO_2 aerogel appears as a white powder (Figure 3a) with an irregular particle morphology and a broad size distribution ranging from 3.78 to 37.1 μm (D90=37.1 μm), as shown in Figs.3(b–c). Its high specific surface area (707.8 m^2/kg) and nanoscale surface roughness (amplitude ≈ 80 nm, Figure 3d) contribute to its effective thermal insulation, which stems from its nanoporous structure that markedly suppresses both solid conduction and gas convection [26,27].

3.4. Experimental Verification of Mix Proportion Design Method and Preliminary Mix Design

A preliminary mix design was conducted using the proposed method based on the upper dry density limit (650kg/m^3). For 1 m^3 AAFC, raw material dosages were calculated: foam from 40 times diluted foaming agent, alkali equivalent 0.1, empirical water-to-binder ratio 0.4, activator modulus 1.5, and curing at 55°C for seven days. The calculation results are listed in Table 6 below.

Table 6. Raw material consumption for the initial mix.

FA (kg/m^3)	Sodium silicate (kg/m^3)	Sodium hydroxide (kg/m^3)	Foam dosage (m^3/m^3)	Water-to-binder Ratio	Additional water dosage (kg/m^3)
396.73	213.45	27.689	0.646	0.4	21.04

3.5. Testing and Results Analysis

The specimens were prepared according to the mix proportion and preparation process, and their relevant properties were tested. The test results are listed in Table 7.

Table 7. Test results of sample performance.

Dry density	Thermal conductivity	Mass water absorption rate	Mechanical properties			Frost resistance (F25)	
ρ (kg/m^3)	λ (W/(m·K))	Wr (%)	f (MPa)	R_f (MPa)	ε (mm/m)	Fc (%)	M_m (%)
632.5	0.1975	57.1%	3.76	0.823	1.432	44.53%	17.36%

 doi:10.20944/preprints202511.1691.v1

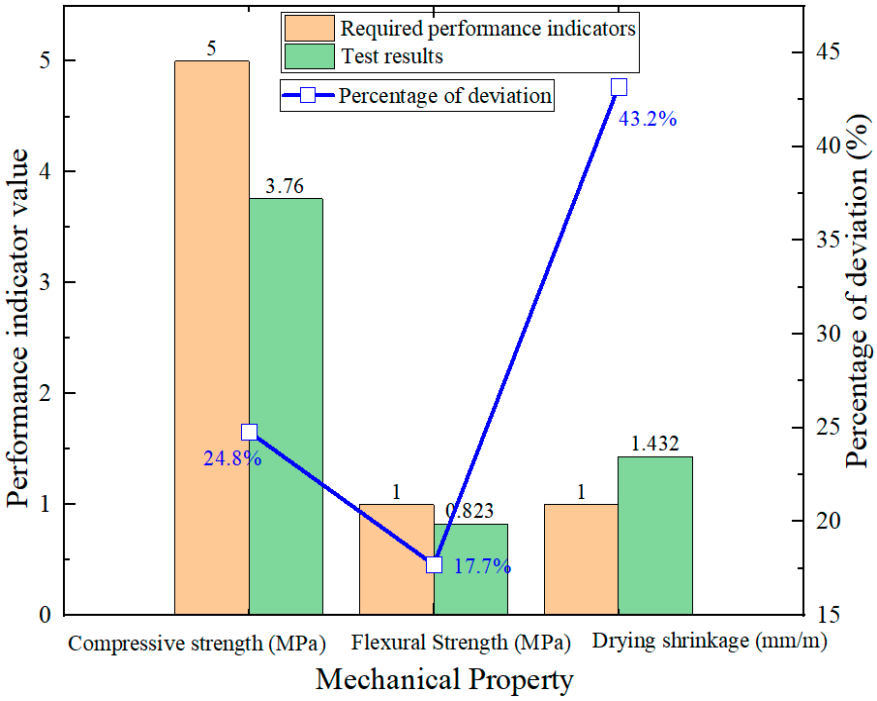

Figure 4. Test results of mechanical properties of preliminary mix ratio samples and deviation rates from the target values.

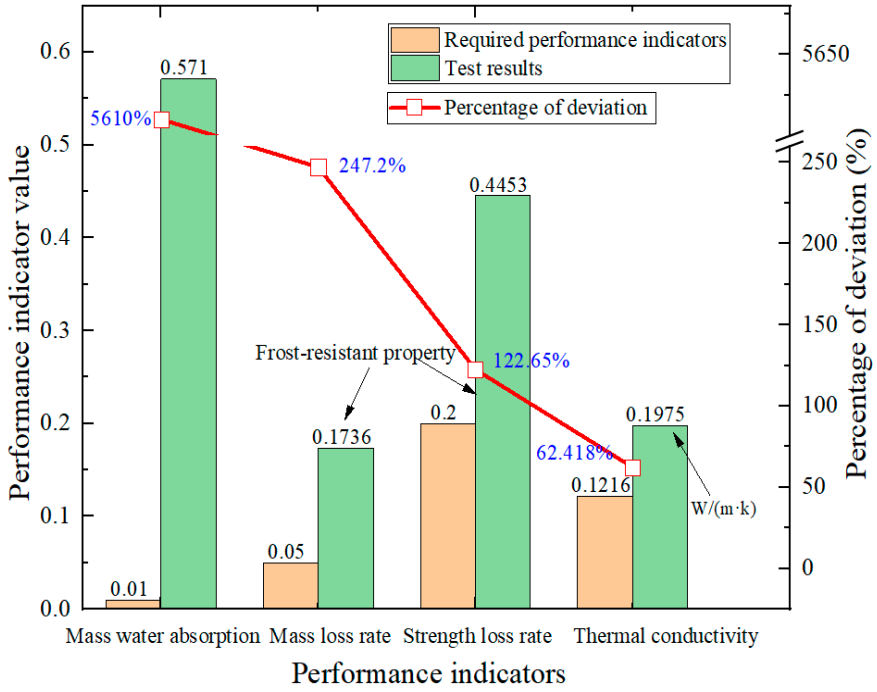

Figure 5. Test results of frost resistance and thermal conductivity of the preliminary mix ratio samples and deviation rates from the target values.

The preliminary mix specimens exhibited deficiencies in several key properties. The compressive strength (3.86 MPa), flexural strength (0.83 MPa), and drying shrinkage (1.432 mm/m) fell short of their target values by 24.8% and 17.7%, respectively, and exceeded their target values by 43.2%. The thermal conductivity reached 0.1975 W/(m·K), exceeding the limit by 62.4%, while the mass water absorption (57.1%) was 11.42 times the target value. Poor water resistance also led to

 doi:10.20944/preprints202511.1691.v1

excessive frost-induced damage, with the strength and mass loss rates surpassing their thresholds by 122.7% and 247.2%, respectively. Consequently, among all the properties evaluated, the feasibility of the design method was validated, but only the dry density met the target requirements, indicating the necessity for comprehensive formulation optimization.

4. Performance Optimization of AAFC Based on Orthogonal Experimental Design

4.1. Performance Optimization Methods and Schemes

Based on the Preliminary Mix, an L_{32} (4^8) orthogonal experiment was designed for comprehensive performance optimization. Eight variables were set at four levels. Considering foam loss, the foam volume dosage was 3.0–4.5times the theoretical value. A foam stabilizer was added at 1–3.5% of the foaming-agent mass. The SiO_2 aerogel was specifically used to enhance the thermal properties and as an internal waterproofing agent to optimize the water resistance. The aerogel dosage was in the range of 2–8 kg/m^3. The calcium hydroxide and waterproofing agent dosages were based on the mass of FA. The vitrified microspheres, basalt fiber, and curing process used fixed parameters of 5% and 1% of FA mass for vitrified microspheres and basalt fiber, respectively.

Table 8. Levels of factors.

Level	Factors							
	Alkali Equivalent (A)	Activator Modulus (B)	Water-to-Binder Ratio (C)	Foam Dosage (D)	Foam Stabilizer Dosage (E)	Aerogel Dosage (F)	Calcium Hydroxide Dosage (G)	Waterproofing Agent Dosage (H)
1	0.08	0.9	0.40	3.0	1%	2	5%	1.5%
2	0.09	1.1	0.45	3.5	1.5%	4	10%	3%
3	0.10	1.3	0.55	4.0	2.5%	6	15%	4.5%
4	0.11	1.5	0.60	4.5	3.5%	8	20%	5.5%

4.2. Orthogonal Experimental Design

An orthogonal experimental design was constructed using the eight variables mentioned above, each at four levels. The factor-level table and orthogonal array are provided below:

Table 9. Orthogonal experimental design table for L_{32} (4^8).

NO.	Factors								
	Alkali Equivalent (A)	Activator Modulus (B)	Water-to-Binder Ratio (C)	Foam Dosage (D)	Foam Stabilizer Dosage (E)	Aerogel Dosage (F)	Calcium Hydroxide Dosage (G)	Waterproofing Agent Dosage (H)	Empty Column (J)
1	1 (0.08)	1 (0.9)	1 (0.40)	1 (3.0)	1 (1%)	1 (2)	1 (5%)	1 (1.5%)	1
2	1	1	2 (0.45)	2 (3.5)	4 (3.5%)	4 (8)	3 (15%)	3 (4.5%)	2
3	1	2 (1.1)	3 (0.55)	4 (4.5)	1	2 (4)	3	4 (5.5%)	3
4	1	2	4 (0.60)	3 (4.0)	4	3 (6)	1	2 (3%)	4
5	1	3 (1.3)	1	3	2 (1.5%)	4	2 (10%)	4	4
6	1	3	2	4	3 (2.5%)	1	4 (20%)	2	3
7	1	4 (1.5)	3	2	2	3	4	1	2
8	1	4	4	1	3	2	2	3	1
9	2 (0.09)	1	3	4	3	4	2	1	4
10	2	1	4	3	2	1	4	3	3
11	2	2	1	1	3	3	4	4	2
12	2	2	2	2	2	2	2	2	1
13	2	3	3	2	4	1	1	4	1
14	2	3	4	1	1	4	3	2	2

 doi:10.20944/preprints202511.1691.v1

15	2	4	1	3	4	2	3	1	3
16	2	4	2	4	1	3	1	3	4
17	3 (0.10)	1	3	1	4	2	4	2	3
18	3	1	4	2	1	3	2	4	4
19	3	2	1	4	4	1	2	3	1
20	3	2	2	3	1	4	4	1	2
21	3	3	3	3	3	3	3	3	2
22	3	3	4	4	2	2	1	1	1
23	3	4	1	2	3	4	1	2	4
24	3	4	2	1	2	1	3	4	3
25	4 (0.11)	1	1	4	2	3	3	2	2
26	4	1	2	3	3	2	1	4	1
27	4	2	3	1	2	4	1	3	4
28	4	2	4	2	3	1	3	1	3
29	4	3	1	2	1	2	4	3	3
30	4	3	2	1	4	3	2	1	4
31	4	4	3	3	1	1	2	2	1
32	4	4	4	4	4	4	4	4	2

Specimens were prepared according to the mix proportions listed in Table 9. The preparation and testing processes are shown in the figure below, and the performance test results for the specimens are listed in Table 10.

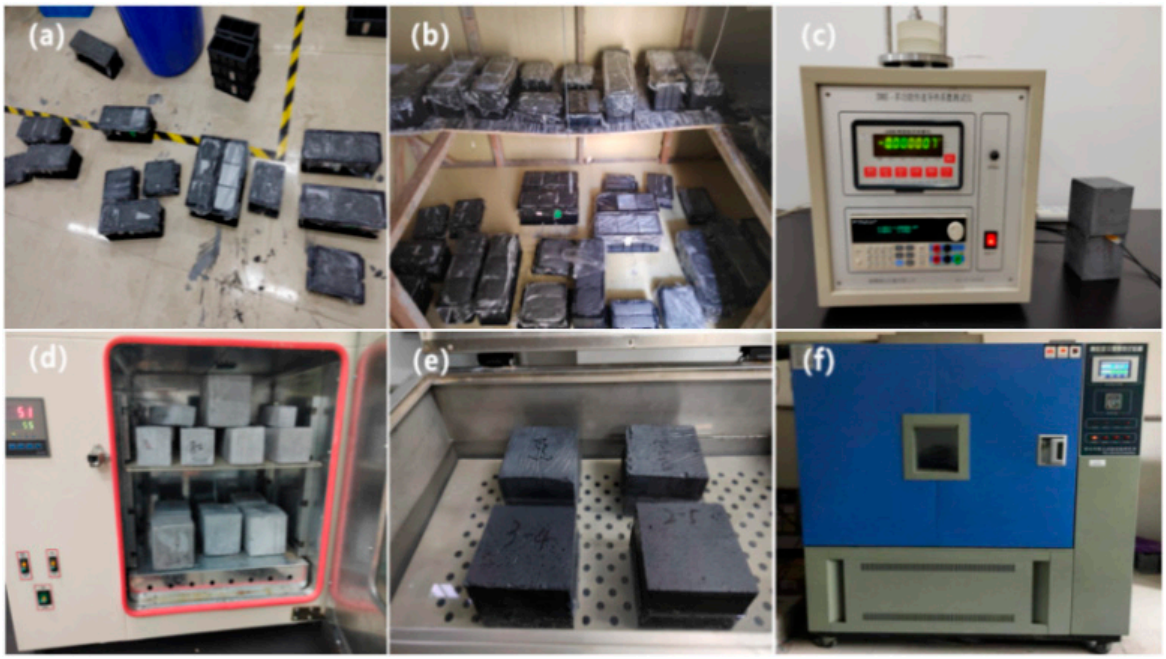

Figure 6. Samples preparation and testing, (a) samples preparation,(b) curing,(c) thermal conductivity measurement,(d) samples drying,(e) water absorption test, (f) frost resistance test.

Table 10. Performance test results of mix ratio samples in orthogonal test.

Index	Bulk Density	Thermal Performance	Water Resistance	Mechanical Properties			Frost Resistance(F25)	
NO.	ρ kg/m^3	λ W/(m·K)	Wr %	f MPa	R_f MPa	ε mm/m	F_c %	M_m %
1	654.82	0.1377	6.50	6.12	1.77	0.849	12.136	2.028
2	633.58	0.0990	4.41	5.47	1.21	0.841	11.124	1.623
3	568.23	0.1001	4.55	5.55	1.32	0.653	11.087	1.597

 doi:10.20944/preprints202511.1691.v1

4	568.34	0.0994	5.50	5.23	1.01	0.747	12.391	2.016
5	581.37	0.0977	4.51	5.47	1.24	0.657	10.553	1.403
6	587.38	0.1138	5.74	5.62	1.38	0.623	12.245	1.981
7	592.23	0.1011	7.21	5.48	1.26	0.841	12.743	2.117
8	588.58	0.0996	4.46	5.31	1.11	0.933	11.135	1.701
9	563.62	0.0980	7.39	5.34	1.15	0.641	13.112	2.243
10	578.95	0.1137	4.69	5.58	1.37	0.738	11.653	1.781
11	655.77	0.1015	4.41	5.62	1.39	0.873	10.127	1.283
12	624.32	0.1022	5.33	6.11	1.85	0.822	11.753	1.887
13	618.79	0.1274	4.61	5.56	1.36	0.847	11.213	1.581
14	580.13	0.0968	5.55	5.64	1.42	1.025	11.873	1.904
15	588.27	0.1002	6.89	5.68	1.44	0.621	12.032	2.104
16	568.57	0.0990	4.81	5.4	1.15	0.608	11.038	1.647
17	621.65	0.1023	5.11	5.55	1.34	0.929	11.214	1.724
18	586.41	0.0988	4.64	5.46	1.18	0.841	10.876	1.549
19	579.69	0.1111	4.86	5.72	1.47	0.537	11.239	1.673
20	577.63	0.0970	4.77	5.24	1.08	0.718	13.037	2.221
21	574.29	0.1012	4.66	5.46	1.20	0.703	11.214	1.732
22	556.83	0.1028	7.41	5.33	1.14	0.704	13.463	2.362
23	643.22	0.0994	4.94	5.78	1.68	0.715	11.463	1.734
24	638.27	0.1304	4.49	6.03	1.78	0.903	10.357	1.352
25	578.61	0.0992	5.77	5.26	1.11	0.554	12.154	2.032
26	581.34	0.0999	4.45	5.47	1.21	0.694	10.443	1.427
27	604.32	0.0954	4.50	5.66	1.44	0.918	11.154	1.683
28	587.73	0.1102	6.55	5.78	1.49	0.835	12.522	2.124
29	645.38	0.1042	4.57	5.72	1.72	0.803	11.223	1.645
30	625.36	0.1008	4.41	5.77	1.52	0.922	12.231	2.102
31	585.66	0.1228	5.70	5.53	1.29	0.724	12.576	2.133
32	564.28	0.0929	4.52	5.27	1.11	0.687	11.137	1.644

As shown in the table, the 32 mix proportion samples exhibited dry densities of 556.83–655.77 kg/m³, with only two slightly exceeding the target. The thermal conductivity ranged from a minimum of 0.0929 W/(m·K) (sample 32) to a maximum of 0.1377 W/(m·K) (sample 1); only samples 1, 13, and 31 marginally exceeded the target. The mechanical properties and freeze-thaw resistance (F25) met these requirements. The lowest mass of water absorption was 4.12% (below the target), although 13 samples exceeded the target. Further analysis is required to identify the optimal mix for achieving the best comprehensive performance.

4.3. Analysis of Influences of Different Factors on Performance

4.3.1. Range Analysis of Test Results

(1) Range Analysis of Dry Density

The range (R) values reveal that the foam content and water-binder ratio are the primary factors influencing dry density, with curves showing the steepest slopes. In contrast, the aerogel content and calcium hydroxide content are secondary factors, while the remaining factors have minimal impacts.

 doi:10.20944/preprints202511.1691.v1

Table 11. Results of dry density range analysis.

Index		Factors								
		A	B	C	D	E	F	G	H	Empty Column
Dry Density (kg/m³)	K_{11}	4774.53	4798.98	4927.13	4968.90	4766.83	4831.29	4796.23	4746.49	4790.03
	K_{12}	4778.42	4766.03	4836.45	4931.66	4754.90	4774.60	4735.01	4789.31	4789.73
	K_{13}	4777.99	4769.53	4728.79	4635.85	4781.93	4749.58	4749.11	4773.36	4795.16
	K_{14}	4772.68	4769.08	4611.25	4567.21	4799.96	4748.15	4823.27	4794.46	4789.77
	k_{11}	596.82	599.87	615.89	621.11	595.85	603.91	599.53	593.31	598.75
	k_{12}	597.30	595.75	604.56	616.46	594.36	596.83	591.88	598.66	598.72
	k_{13}	597.25	596.19	591.10	579.48	597.74	593.70	593.64	596.67	599.40
	k_{14}	596.59	596.14	576.41	570.90	600.00	593.52	602.91	599.31	598.72
R		0.72	4.12	39.49	50.21	5.63	10.39	11.03	6.00	0.68
Optimal Level		2	1	1	1	4	1	4	4	

Note: K_{ij} represents the sum of test results corresponding to level j in any factor column under the performance index i. k_{ij} denotes the average value of test results for level number j in any factor column.

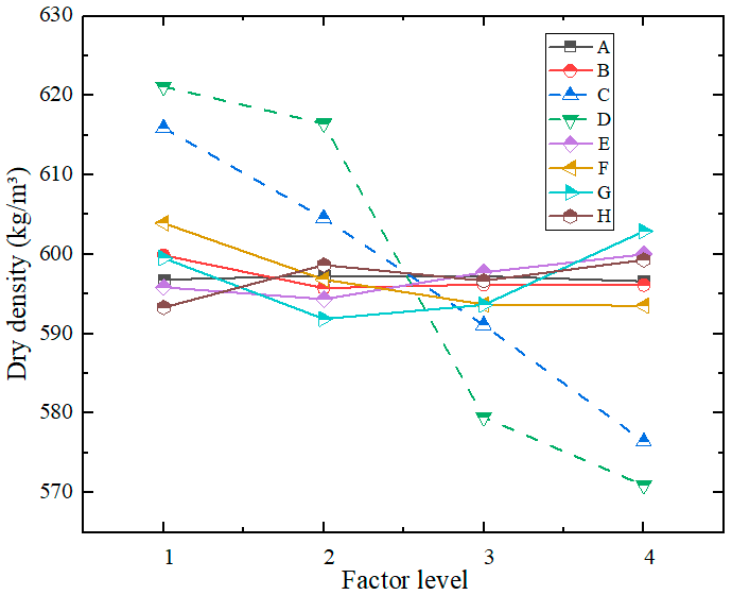

Figure 7. Dry density of AAFC varies with the levels of various factors.

(2) Range Analysis of Thermal Conductivity

The thermal conductivity decreased with increasing foam and aerogel content. The curve slope for aerogel content was the steepest, indicating the greatest influence magnitude, significantly exceeding the other factors. This demonstrates that aerogel, as a super-insulating material, can remarkably reduce the thermal conductivity of FC. Foam content is the next most influential factor, and is well documented[38–40]. Other factors exerted minimal effects.

 doi:10.20944/preprints202511.1691.v1

Table 12. Results of thermal conductivity range analysis.

Index		Factors								
		A	B	C	D	E	F	G	H	Empty Column
Thermal Conductivity (W/(m·K))	K_{21}	0.8484	0.8486	0.8510	0.8645	0.8564	0.9671	0.8610	0.8478	0.8035
	K_{22}	0.8388	0.8169	0.8421	0.8422	0.8426	0.8113	0.8310	0.8358	0.7887
	K_{23}	0.8430	0.8447	0.8484	0.8319	0.8236	0.8010	0.8371	0.8233	0.8049
	K_{24}	0.8254	0.8454	0.8141	0.8170	0.8330	0.7761	0.8265	0.8486	0.7885
	k_{21}	0.1060	0.1061	0.1064	0.1081	0.1071	0.1209	0.1076	0.1060	0.1004
	k_{22}	0.1049	0.1021	0.1053	0.1053	0.1053	0.1014	0.1039	0.1045	0.0986
	k_{23}	0.1054	0.1056	0.1060	0.1040	0.1029	0.1001	0.1046	0.1029	0.1006
	k_{24}	0.1032	0.1057	0.1018	0.1021	0.1041	0.0970	0.1033	0.1061	0.0986
R		0.0029	0.0040	0.0046	0.0059	0.0041	0.0239	0.0043	0.0032	0.0021
Optimal Level		4	2	4	4	3	4	4	3	

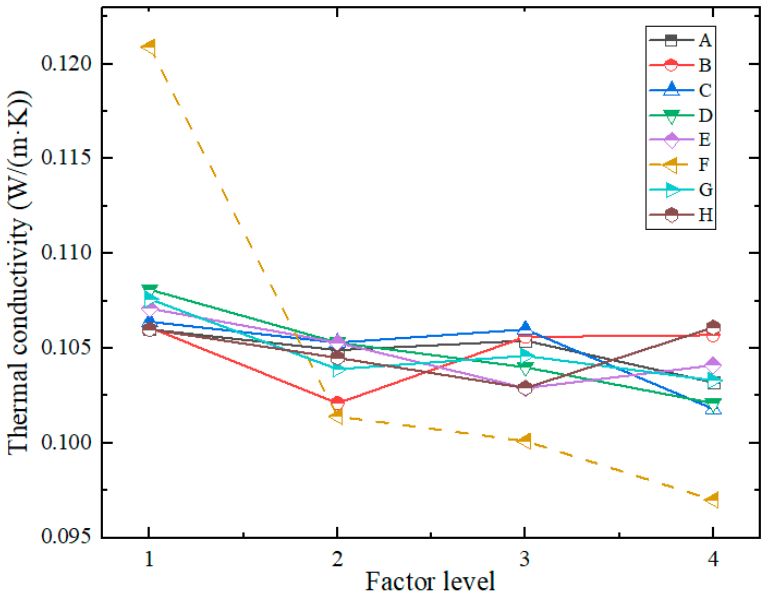

Figure 8. Thermal conductivity of AAFC varies with the levels of various factors.

(3) Mass Water Absorption Rate

Analysis of the range values (R) and curves in Figure 9 shows that the waterproofing agent dosage was the most significant factor affecting the mass water absorption rate, which decreased significantly with increasing dosage. Compared with previous studies, the waterproofing performance has been effectively improved[9]. Foam content was the next most influential factor, although the range value (R) of the former was approximately 2.7 times that of the latter. Factors such as activator modulus, water-binder ratio, and calcium hydroxide content showed negligible effects.

 doi:10.20944/preprints202511.1691.v1

Table 13. Results of mass water absorption rate range analysis.

Index		Factors								
		A	B	C	D	E	F	G	H	Empty Column
Mass Water Absorption Rate(%)	K_{31}	107.2	107.4	106.12	98.576	102.7	107.85	106.8	127.835	108.301
	K_{32}	109.2	101.1	96.030	105.64	109.7	106.91	103.2	109.090	103.271
	K_{33}	102.1	103.6	109.31	102.95	106.4	103.55	107.1	92.385	106.46
	K_{34}	101.1	107.5	108.32	112.61	100.7	101.47	102.5	90.473	101.751
	k_{31}	13.40	13.42	13.265	12.322	12.84	13.481	13.35	15.979	13.538
	k_{32}	13.65	12.64	12.004	13.205	13.72	13.364	12.90	13.636	12.909
	k_{33}	12.77	12.95	13.664	12.869	13.31	12.944	13.39	11.548	13.308
	k_{34}	12.64	13.44	13.540	14.077	12.59	12.684	12.82	11.309	12.719
R		1.003	0.802	1.660	1.755	1.124	0.798	0.576	4.670	0.819
Optimal Level		4	2	2	1	4	4	4	4	

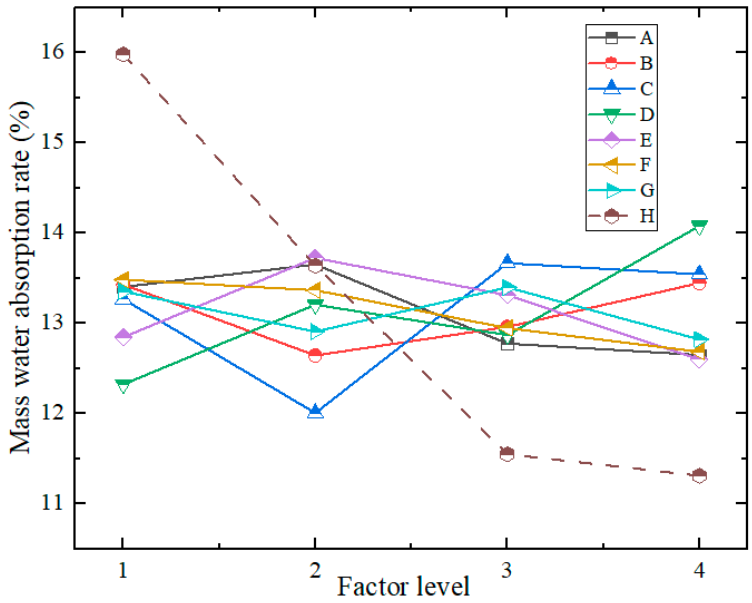

Figure 9. Water absorption of AAFC varies with the levels of various factors.

(4) Mechanical Properties

Analysis of the range values (R) for compressive and flexural strengths (Tables 14–16) reveals that aerogel content, foam content, and water-binder ratio are the three most influential factors. The foam stabilizer dosage had the least significant effect on the compressive strength, while calcium hydroxide content had a relatively minor influence on the flexural strength. As shown in the curves in Figure 9, both the compressive and flexural strengths decrease significantly with increasing foam content, aerogel content, and water-binder ratio. A higher foam content introduces more air bubbles into the solid matrix, which increases the porosity and degrades the mechanical properties. The hydration products (C(N)-A-S-H) are critical for the strength development of AAFC[41,42]. Appropriate addition of calcium hydroxide can increase the proportion of C-A-S-H in the hydration products[43], thereby improving the mechanical properties. The effect of foam stabilizer dosage on the mechanical properties follows a pattern of first decreased and then increased. As a surfactant, an appropriate amount of stabilizer improves the stability of bubble membranes, prolongs their rupture half-life, and controls the bubble uniformity, size, and quantity in the slurry to enhance the mechanical properties[44].

 doi:10.20944/preprints202511.1691.v1

Table 14. Results of compressive strength range analysis.

Index		Factors								
		A	B	C	D	E	F	G	H	Empty Column
Compressive Strength (MPa)	K_{41}	44.25	44.25	45.37	45.7	44.66	46.49	45.1	44.74	45.15
	K_{42}	44.93	44.36	44.56	45.36	44.37	44.17	44.16	44.17	45.44
	K_{43}	44.57	45.12	44.68	43.66	44.38	43.68	44.87	44.32	45.51
	K_{44}	44.46	44.48	43.6	43.49	44.8	43.87	44.08	44.98	45.12
	k_{41}	5.531	5.531	5.671	5.713	5.583	5.811	5.638	5.593	5.644
	k_{42}	5.616	5.545	5.570	5.670	5.546	5.521	5.520	5.521	5.680
	k_{43}	5.571	5.640	5.585	5.458	5.548	5.460	5.609	5.540	5.689
	k_{44}	5.558	5.560	5.450	5.436	5.600	5.484	5.510	5.623	5.640
R		0.085	0.109	0.221	0.276	0.054	0.351	0.128	0.101	0.049
Optimal Level		2	3	1	1	4	1	1	4	

Table 15. Results of flexural strength range analysis.

Index		Factors								
		A	B	C	D	E	F	G	H	Empty Column
Flexural Strength (MPa)	K_{51}	10.30	10.34	11.82	11.76	10.94	11.91	10.76	10.83	11.21
	K_{52}	11.13	11.04	11.18	11.76	11.18	11.13	10.81	11.08	11.31
	K_{53}	10.88	10.97	10.36	9.84	10.61	9.82	10.96	10.67	11.33
	K_{54}	10.88	10.83	9.83	9.82	10.46	10.32	10.65	10.60	10.99
	k_{51}	1.287	1.293	1.477	1.469	1.367	1.489	1.345	1.354	1.401
	k_{52}	1.391	1.381	1.397	1.4701	1.398	1.391	1.351	1.385	1.414
	k_{53}	1.359	1.371	1.295	1.230	1.326	1.228	1.370	1.334	1.416
	k_{54}	1.360	1.354	1.228	1.228	1.307	1.290	1.331	1.324	1.373
R		0.104	0.088	0.249	0.243	0.090	0.261	0.039	0.061	0.043
Optimal Level		2	2	1	2	2	1	3	2	

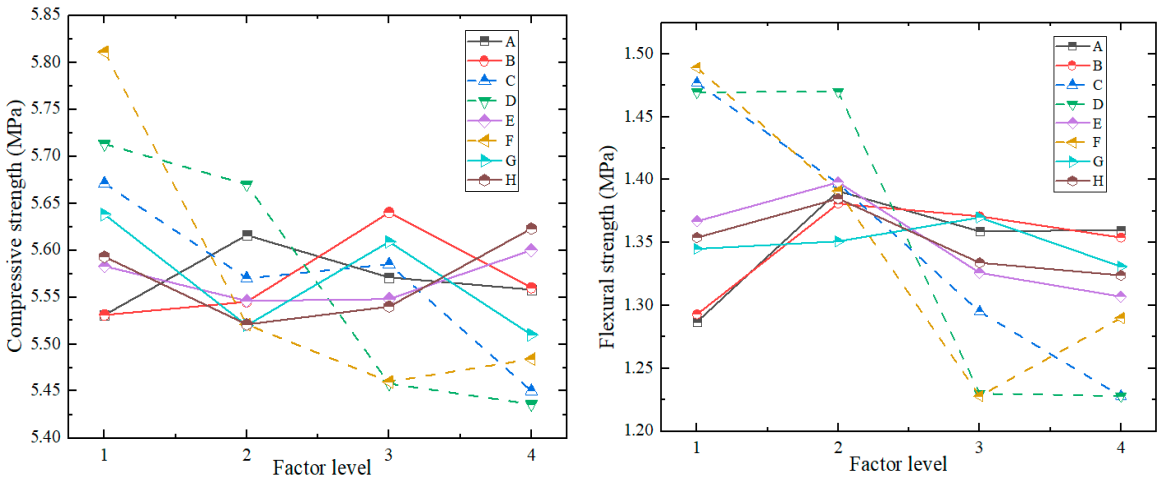

(a) compressive strength (b) flexural strength

Figure 10. Mechanical properties of AAFC varies with the levels of various factors.

Range analysis indicated that foam content was the most dominant factor influencing drying shrinkage, followed by the water–binder ratio, with other factors having negligible effects. As shown

 doi:10.20944/preprints202511.1691.v1

in Figure 11, the drying shrinkage decreases nearly linearly with increasing foam content, which is attributable to the increased porosity, which reduces the solid phase fraction and thus the autogenous shrinkage of the AA matrix. In contrast, drying shrinkage increases with the water–binder ratio; higher ratios improve workability but also increase macroporosity and connectivity, accelerating moisture loss and capillary evaporation. The resulting capillary pressure difference further intensifies the shrinkage stress.

Table 16. Results of drying shrinkage range analysis.

Index		Factors								
		A	B	C	D	E	F	G	H	Empty Column
Drying Shrinkage (mm/m)	K_{61}	6.144	6.087	5.609	7.352	6.221	6.056	6.082	6.131	6.11
	K_{62}	6.175	6.103	6.131	6.545	6.137	6.159	6.077	6.139	6.103
	K_{63}	6.05	6.284	6.256	5.602	6.017	6.089	6.135	6.081	6.105
	K_{64}	6.137	6.032	6.51	5.007	6.131	6.202	6.212	6.155	6.049
	k_{61}	0.768	0.761	0.701	0.919	0.778	0.757	0.7603	0.766	0.764
	k_{62}	0.772	0.763	0.766	0.818	0.767	0.770	0.7596	0.767	0.763
	k_{63}	0.756	0.786	0.782	0.700	0.752	0.761	0.767	0.760	0.763
	k_{64}	0.767	0.754	0.814	0.626	0.766	0.775	0.777	0.769	0.756
R		0.016	0.031	0.113	0.293	0.026	0.018	0.017	0.009	0.008
Optimal Level		3	4	1	4	3	1	2	3	

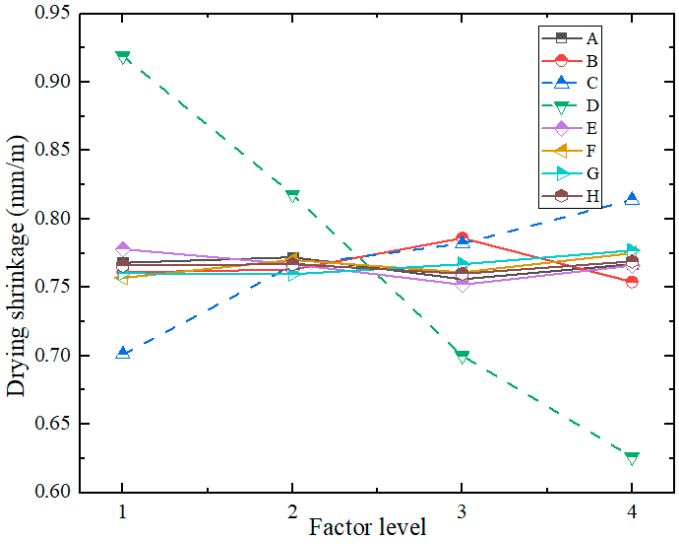

Figure 11. Drying shrinkage of AAFC varies with the level of various factors.

(5) Frost Resistance

The range calculation and analysis results of the strength loss rate and mass loss rate are listed in Tables 17–18:

 doi:10.20944/preprints202511.1691.v1

Table 17. Results of strength loss rate range analysis.

Index		Factors								
		A	B	C	D	E	F	G	H	Empty Column
Strength Loss Rate (%)	K_{71}	93.414	92.712	90.927	90.227	93.846	93.941	93.301	101.276	93.958
	K_{72}	92.801	93.310	92.228	92.917	93.830	92.350	93.475	95.669	93.409
	K_{73}	92.863	94.015	94.313	93.899	92.261	92.774	92.363	89.780	93.333
	K_{74}	93.440	92.481	95.050	95.475	92.581	93.453	93.379	85.793	93.818
	k_{71}	11.677	11.589	11.366	11.278	11.731	11.743	11.663	12.660	11.745
	k_{72}	11.600	11.664	11.529	11.615	11.729	11.544	11.684	11.959	11.676
	k_{73}	11.608	11.752	11.789	11.737	11.533	11.597	11.545	11.223	11.667
	k_{74}	11.680	11.560	11.881	11.934	11.573	11.682	11.672	10.724	11.727
R		0.080	0.192	0.515	0.656	0.198	0.199	0.139	1.935	0.078
Optimal Level		2	4	1	1	3	2	3	4	

Table 18. Results of mass loss rate range analysis.

Index		Factors								
		A	B	C	D	E	F	G	H	Empty Column
Mass Loss Rate (%)	K_{81}	14.466	14.407	13.902	13.777	14.724	14.653	14.478	17.301	14.523
	K_{82}	14.43	14.484	14.24	14.26	14.617	14.447	14.691	15.411	14.556
	K_{83}	14.347	14.71	14.81	14.817	14.225	14.478	14.468	13.485	14.308
	K_{84}	14.79	14.432	15.081	15.179	14.467	14.455	14.396	11.836	14.377
	k_{81}	1.808	1.801	1.738	1.722	1.841	1.832	1.810	2.163	1.815
	k_{82}	1.804	1.811	1.780	1.783	1.827	1.806	1.836	1.926	1.820
	k_{83}	1.793	1.839	1.851	1.852	1.778	1.810	1.809	1.686	1.789
	k_{84}	1.849	1.804	1.885	1.897	1.808	1.807	1.800	1.480	1.797
R		0.055	0.038	0.147	0.175	0.062	0.026	0.037	0.683	0.031
Optimal Level		3	1	1	1	3	2	4	4	

By comparing the range values (R), it can be seen that the three most influential factors on the freezing resistance of the AAFC are, in order: waterproofing agent dosage, foam content, and water-binder ratio. The other factors had relatively minor effects.

The dosage of the waterproofing agent demonstrated the most significant effect on frost resistance, with both the strength and mass loss rates decreasing approximately linearly as its content increased. This improvement was attributed to the reduction in water absorption, which mitigated the 9% volumetric expansion of water upon freezing and the resultant frost-heave pressure within the pores. In contrast, increased foam content reduces frost resistance by increasing porosity, coarsening pore structures, and thinning pore walls, thereby elevating water absorption and exacerbating frost-induced damage. Similarly, a higher water–binder ratio diminishes frost resistance by promoting slurry fluidity and altering pore characteristics, leading to internal stress differences between saturated and unsaturated zones during freeze–thaw cycles.

 doi:10.20944/preprints202511.1691.v1

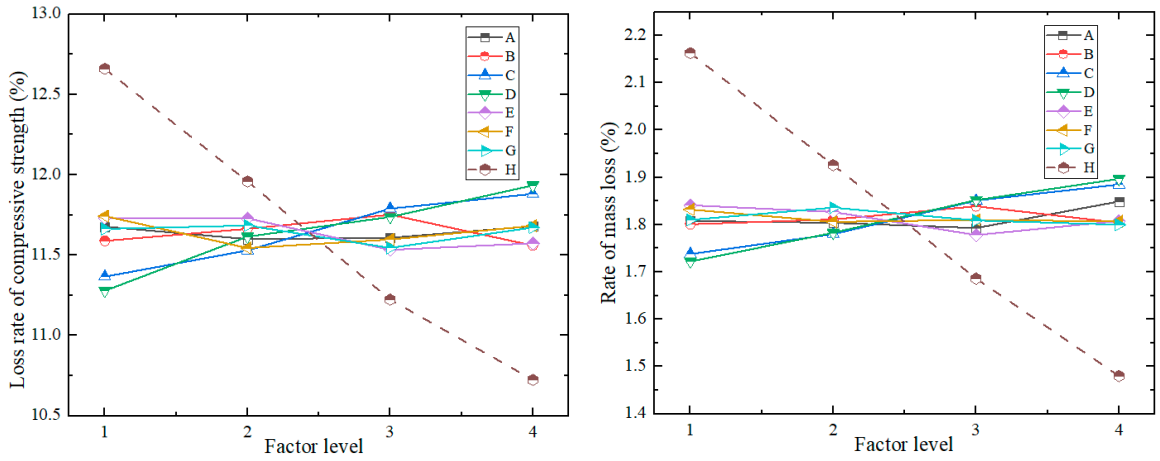

(a) strength loss rate (b) mass loss rate

Figure 12. Frost resistance of AAFC varies with the levels of various factors.

4.3.2. Analysis of Variance (ANOVA) of Test Results

Range analysis of orthogonal test results can effectively determine the primary and secondary orders of influencing factors, but it cannot distinguish data fluctuations caused by changes in test conditions and errors, nor evaluate the significance level of the influencing factors. Therefore, ANOVA was conducted. The significance of the influence of each factor can be determined by constructing an F-statistic for the F-test.

Table 19. Results of variance analysis of orthogonal test.

Index	Source of variance	Sum of squared deviations		Degree of freedom	Mean square Ms	F Value	Significance
Dry Density (kg/m³)	A	SS_A	2.870	3	0.957	0.044	
	B	SS_B	89.649	3	29.883	1.365	
	C	SS_C	6983.224	3	2327.741	106.320	**
	D	SS_D	15584.462	3	5194.821	237.275	**
	E	SS_E	142.314	3	47.438	2.167	
	F	SS_F	566.568	3	188.856	8.626	(*)
	G	SS_G	630.865	3	210.288	9.605	*
	H	SS_H	174.463	3	58.154	2.656	
	Error E	SS_E	65.681	3	21.894		
	Sum	SS_T	24240.096	31			
Thermal Conductivity (W/(m·K))	A	SS_A	3.59384E-05	3	1.198E-05	2.7289	
	B	SS_B	8.13828E-05	3	2.713E-05	6.1796	(*)
	C	SS_C	0.000107308	3	3.577E-05	8.1481	(*)
	D	SS_D	0.000149903	3	4.997E-05	11.3825	*
	E	SS_E	7.37212E-05	3	2.457E-05	5.5978	(*)
	F	SS_F	0.002821489	3	0.0009405	214.2426	**
	G	SS_G	8.81847E-05	3	2.939E-05	6.6961	(*)
	H	SS_H	5.35474E-05	3	1.785E-05	4.0660	
	Error E	SS_E	1.32E-05	3	4.39E-06		

 doi:10.20944/preprints202511.1691.v1

	Sum	SS_T	0.003425	31			
Mass Water Absorption Rate (%)	A	SS_A	18.2856	3	6.0952	8.5416	(*)
	B	SS_B	16.3877	3	5.4626	7.6550	(*)
	C	SS_C	45.2873	3	15.0958	21.1547	*
	D	SS_D	57.3406	3	19.1135	26.7850	*
	E	SS_E	31.0806	3	10.3602	14.5184	*
	F	SS_F	12.6851	3	4.2284	5.9255	(*)
	G	SS_G	9.5971	3	3.1990	4.4830	
	H	SS_H	80.2010	3	26.7337	37.4636	**
	Error E	SS_E	2.141	3	0.714		
	Sum	SS_T	273.0056	31			
Compressive Strength (MPa)	A	SS_A	0.0335	3	0.0112	9.8946	*
	B	SS_B	0.0436	3	0.0145	12.8866	*
	C	SS_C	0.2581	3	0.0860	76.2713	**
	D	SS_D	0.3975	3	0.1325	117.4714	**
	E	SS_E	0.0165	3	0.0055	4.8859	
	F	SS_F	0.4868	3	0.1623	143.8448	**
	G	SS_G	0.0281	3	0.0094	8.3063	(*)
	H	SS_H	0.0304	3	0.0101	8.9712	(*)
	Error E	SS_E	0.0034	3	0.0011		
	Sum	SS_T	1.2979	31			
Flexural Strength (MPa)	A	SS_A	0.2966	3	0.0989	29.0104	*
	B	SS_B	0.1443	3	0.0481	14.1092	*
	C	SS_C	0.3822	3	0.1274	37.3773	**
	D	SS_D	0.3745	3	0.1248	36.6244	**
	E	SS_E	0.2225	3	0.0742	21.7644	*
	F	SS_F	0.4065	3	0.1355	39.7534	**
	G	SS_G	0.0900	3	0.0300	8.7988	(*)
	H	SS_H	0.0943	3	0.0314	9.2191	(*)
	Error E	SS_E	0.0102	3	3.41E-03		
	Sum	SS_T	2.0210	31			
Drying Shrinkage (mm/m)	A	SS_A	0.0349	3	0.0116	2.0999	
	B	SS_B	0.1196	3	0.0399	7.2035	(*)
	C	SS_C	0.1311	3	0.0437	7.8952	(*)
	D	SS_D	0.4267	3	0.1422	25.6941	*
	E	SS_E	0.0486	3	0.0162	2.9261	
	F	SS_F	0.0413	3	0.0138	2.4885	
	G	SS_G	0.0382	3	0.0127	2.3019	
	H	SS_H	0.0295	3	0.0098	1.7760	
	Error E	SS_E	0.0166	3	0.0055		
	Sum	SS_T	0.8866	31			

 doi:10.20944/preprints202511.1691.v1

Strength Loss Rate (%)	A	SS_A	7.2638	3	2.4213	5.0263	
	B	SS_B	11.8639	3	3.9546	8.2094	(*)
	C	SS_C	20.5288	3	6.8429	14.2052	*
	D	SS_D	21.6072	3	7.2024	14.9514	*
	E	SS_E	14.2014	3	4.7338	9.8269	*
	F	SS_F	12.1380	3	4.0460	8.3990	(*)
	G	SS_G	9.3936	3	3.1312	6.5000	(*)
	H	SS_H	45.0139	3	15.0046	31.1481	**
	Error E	SS_E	1.4452	3	0.4817		
	Sum	SS_T	143.4557	31			
Mass Loss Rate (%)	A	SS_A	0.2816	3	0.0939	8.4316	(*)
	B	SS_B	0.2977	3	0.0992	8.9154	(*)
	C	SS_C	0.9241	3	0.3080	27.6718	*
	D	SS_D	1.0934	3	0.3645	32.7423	**
	E	SS_E	0.3931	3	0.1310	11.7724	*
	F	SS_F	0.1694	3	0.0565	5.0716	
	G	SS_G	0.2258	3	0.0753	6.7621	(*)
	H	SS_H	1.9874	3	0.6625	59.5113	**
	Error E	SS_E	0.3339	3	0.1113		
	Sum	SS_T	5.7064	31			

The range and variance analysis results in Table 19 show good consistency. A comprehensive analysis of both methods led to the following conclusions.

(1) Foam content significantly affects all properties, reducing density and thermal conductivity, but increasing water absorption and shrinkage while compromising mechanical and frost resistance, requiring careful optimization.

(2) The aerogel content exhibited an extremely significant effect on thermal performance. Combining the increased aerogel content with moderately reduced foam content simultaneously enhanced the thermal and mechanical properties.

(3) The water-binder ratio significantly influences the mechanical properties and density, with significant effects on water absorption and frost resistance. Its complex effects necessitate careful optimization.

(4) Calcium hydroxide moderately improved the mechanical properties through an initial-decrease-then-increase pattern, while showing negligible effects on other parameters.

(5) The waterproofing agent significantly enhances the water resistance and frost durability, slightly improves the mechanical properties, and minimally affects the thermal and density characteristics.

4.3.3. Microscopic Analysis

(1) SEM

The variations in the mix proportions resulted in significant changes in the micro-morphologies of the specimens (Figure 13). Among the six groups of specimens, both pore size and porosity generally showed an increasing trend: Specimen S3 had the largest pore size, along with the smallest thermal conductivity and dry density, whereas the opposite was true for Specimen S1.This trend shows a strong correlation with the pore size and characteristics[45,46]. This indicated that the foam

 doi:10.20944/preprints202511.1691.v1

content and water-to-binder ratio exerted a significant influence on the pore structure. Although Specimens S5 and S11 differ in water-to-binder ratio and foam content, their low thermal conductivity, attributed to the high aerogel content, confirms that the aerogel is a key influencing factor. SEM images reveal that Specimen S3 features high porosity and thin pore walls, whereas Specimen S11, with a higher dosage of foam stabilizer, exhibited fewer interconnected pores and more uniform pore sizes[47]. The random dispersion of basalt fibers is conducive to enhancing the mechanical properties, and the absence of independent FA particles is consistent with the reaction mechanism of alkali-activated FA.

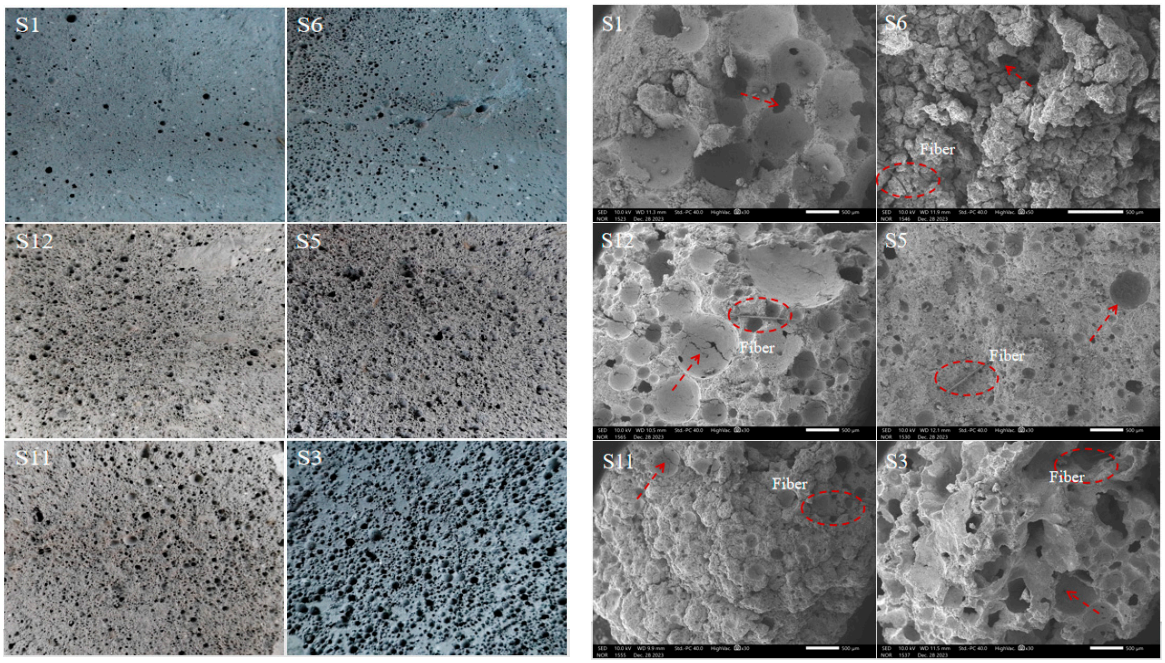

(a) Changes in the appearance of samples with different formulations

(b) Changes in the microstructure of samples with different formulations(SEM)

Figure 13. Morphologies of samples with different mix ratios.

(2) FTIR

The analysis indicates that the wavenumber range of 1000–1040 cm < B-> ¹ corresponds to the asymmetric stretching vibration peak of Si-O-X (Na/Al), which is the most prominent characteristic absorption peak of alkali-activated FA cementitious materials[48]. The absorption peak intensities vary among the six groups of specimens: a stronger and sharper peak suggests a higher content of hydrated sodium (calcium) aluminosilicate (C,N-A-S-H) in the reaction products, which is beneficial for enhancing the mechanical properties of FC[49,50]. Additionally, compared with the infrared spectrum of FA, the characteristic peak of Si-O-X (Na/Al) in the products shifted to a lower wavenumber, a feature that reflects the gradual increase in C,N-A-S-H gel products[29,31]. Moreover, due to differences in alkali concentration among systems with various mix proportions, there are certain variations in the extent of the peak shift. The peak at 1430 cm < st > ¹ corresponds to the asymmetric stretching vibration of carbonate, with the peak of S11 being the strongest. Because S11 had the highest alkali equivalent among the six mix proportions, the system of this mix proportion exhibited strong alkalinity, indicating the maximum formation of carbonate. Furthermore, there are two characteristic peaks at 3433 cm^{-1} and 1630 cm^{-1}, which correspond to the bending vibration peak of H-O-H bonds, among which the peak at 1630 cm^{-1} is the characteristic peak of bound water in cementitious materials[51].

 doi:10.20944/preprints202511.1691.v1

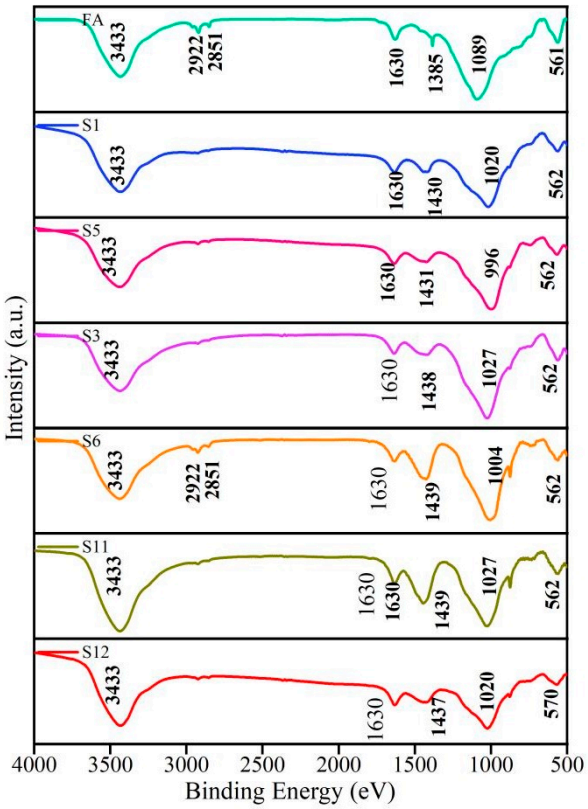

Figure 14. FTIR diagram of samples with different mix ratios.

4.4. Determination of Optimal Mix Proportion for AAFC

4.4.1. Mix Proportion Optimization Method

Both range and variance analyses are single-factor analysis methods that cannot determine the optimal mix proportion under multi-factor conditions in orthogonal experiments. The matrix analysis method can objectively conduct a comprehensive analysis of multifactor and multiindex systems and calculate the weights of each factor level. Therefore, matrix analysis was used to determine the optimal mix proportion for the AAFC.

Based on the orthogonal experimental scheme and the performance index system of the AAFC, a three-layer hierarchical structure model was constructed, including the index, factor, and level layers. The model consists of eight factors with four levels each, and eight performance indicators were investigated. The constructed structural model is presented in the following table:

Table 20. Orthogonal test of AAFC data structure model.

Index Layer	Performance Indicators												
Factor Layer	Factor A				Factor B				···	Factor H			
Level Layer	A_1	A_2	···	A_4	B_1	B_2	···	B_4	···	H_1	H_2	···	H_4

Index Layer Matrix: The average value of the test index for factor X_i at the j level is defined as m_{ij}. For indicators in which larger values indicate better performance, $M_{ij}=m_{ij}$; for indicators in which smaller values are preferable, $M_{ij}=1/m_{ij}$. The established index matrix is expressed by Eq.8:

 doi:10.20944/preprints202511.1691.v1

$$M=\begin{bmatrix} M_{11} & 0 & 0 & \cdots & 0 \\ M_{12} & 0 & 0 & \cdots & 0 \\ \cdots & \cdots & \cdots & \cdots & \cdots \\ M_{1m} & 0 & 0 & \cdots & 0 \\ 0 & M_{21} & 0 & \cdots & 0 \\ 0 & M_{22} & 0 & \cdots & 0 \\ \cdots & \cdots & \cdots & \cdots & \cdots \\ 0 & M_{2m} & 0 & \cdots & 0 \\ 0 & 0 & 0 & \cdots & 0 \\ 0 & 0 & 0 & \cdots & M_{l1} \\ 0 & 0 & 0 & \cdots & M_{l1} \\ \cdots & \cdots & \cdots & \cdots & \cdots \\ 0 & 0 & 0 & \cdots & M_{lm} \end{bmatrix} \tag{8}$$

$$T_i=\frac{1}{\sum_{j=1}^{m} M_{ij}}$$

Factor Layer Matrix: Let , the factor matrix is established as shown in Eq.9:

$$T=\begin{bmatrix} T_1 & 0 & \cdots & 0 \\ 0 & T_2 & \cdots & 0 \\ \cdots & \cdots & \cdots & \cdots \\ 0 & 0 & \cdots & T_l \end{bmatrix} \tag{9}$$

$$S_i=\frac{s_i}{\sum_{i=1}^{l} s_i}$$

Level Layer Matrix: Calculate the range S_i of factor A_i, Let , the factor matrix is established as shown in Eq.10:

$$S=\begin{bmatrix} S_1 \\ S_2 \\ \cdots \\ S_l \end{bmatrix} \tag{10}$$

Weight Matrix: For the weight matrix of the factors influencing the test indices $\omega_i = M_i T_i S_i$, ω_i^T can be expressed as follows:

$$\omega_i^T=[\omega_1, \omega_2, \mathrm{L}, \omega_\mathrm{m}] \tag{11}$$

The total weight matrix was obtained by averaging the sum of the weight matrices for each factor ω_i, as shown in Eq.12:

$$\omega^\mathrm{T} = (\omega_1^\mathrm{T} + \omega_2^\mathrm{T} + \mathrm{L} + \omega_x^\mathrm{T})/l \tag{12}$$

 doi:10.20944/preprints202511.1691.v1

4.4.2. Analysis and Determination of Optimal Mix Proportion

The weight matrix for eight performance indicators, including dry density, was calculated based on the established three-layer hierarchical structure model. For five indicators (thermal conductivity, mass water absorption rate, drying shrinkage, strength loss rate, and mass loss rate), smaller values were preferable; therefore, $M_{ij}=1/m_{ij}$ was adopted. For dry density, compressive strength, and flexural strength (where larger values are preferable), $M_{ij}=1/m_{ij}$ was used. The calculation results based on this method are listed in the following table:

Table 21. Results of matrix analysis.

Factor	ρ	λ	Wr	f	R_f	ε	F_c	M_m	Total
A1	0.00140	0.00135	0.01978	0.01592	0.02180	0.00745	0.00508	0.01134	0.01052
A2	0.00140	0.00137	0.01942	0.01617	0.02356	0.00741	0.00511	0.01137	0.01073
A3	0.00140	0.00136	0.02076	0.01604	0.02303	0.00756	0.00511	0.01143	0.01084
A4	0.00140	0.00139	0.02096	0.01600	0.02305	0.00745	0.00508	0.01109	0.01080
B1	0.00803	0.00186	0.01579	0.02038	0.01855	0.01515	0.01230	0.00779	0.01248
B2	0.00808	0.00194	0.01677	0.02043	0.01981	0.01511	0.01222	0.00774	0.01276
B3	0.00808	0.00187	0.01637	0.02078	0.01967	0.01468	0.01213	0.00762	0.01265
B4	0.00808	0.00187	0.01577	0.02048	0.01942	0.01529	0.01233	0.00777	0.01263
C1	0.07494	0.00217	0.03304	0.04251	0.05997	0.05865	0.03370	0.03138	0.04204
C2	0.07635	0.00219	0.03651	0.04175	0.05673	0.05366	0.03322	0.03063	0.04138
C3	0.07809	0.00217	0.03208	0.04186	0.05258	0.05259	0.03249	0.02945	0.04016
C4	0.08008	0.00226	0.03237	0.04085	0.04987	0.05053	0.03224	0.02892	0.03964
D1	0.09443	0.00275	0.03761	0.05346	0.05818	0.11434	0.04322	0.03764	0.05520
D2	0.09514	0.00283	0.03510	0.05306	0.05820	0.12844	0.04197	0.03636	0.05639
D3	0.10122	0.00286	0.03601	0.05107	0.04871	0.15006	0.04153	0.03500	0.05831
D4	0.10274	0.00291	0.03292	0.05088	0.04859	0.16789	0.04085	0.03416	0.06012
E1	0.01105	0.00192	0.02314	0.01016	0.02017	0.01200	0.01255	0.01255	0.01294
E2	0.01108	0.00195	0.02166	0.01010	0.02063	0.01217	0.01255	0.01264	0.01285
E3	0.01102	0.00199	0.02233	0.01010	0.01956	0.01241	0.01277	0.01299	0.01290
E4	0.01098	0.00197	0.02360	0.01019	0.01929	0.01218	0.01272	0.01277	0.01296
F1	0.00190	0.01186	0.01630	0.06497	0.05237	0.00878	0.01275	0.00527	0.02177
F2	0.00189	0.01171	0.01579	0.06570	0.05934	0.00868	0.01280	0.00528	0.02265
F3	0.00187	0.00983	0.01565	0.06915	0.06352	0.00882	0.01259	0.00520	0.02333
F4	0.00190	0.01225	0.01663	0.06525	0.05503	0.00862	0.01265	0.00527	0.02220
G1	0.00163	0.00206	0.01138	0.02422	0.00880	0.00805	0.00895	0.00755	0.00908
G2	0.00164	0.00207	0.01181	0.02384	0.00868	0.00813	0.00884	0.00743	0.00906
G3	0.00162	0.00200	0.01142	0.02435	0.00864	0.00812	0.00886	0.00754	0.00907
G4	0.00161	0.00209	0.01189	0.02380	0.00855	0.00795	0.00885	0.00759	0.00904
H1	0.00167	0.00150	0.07587	0.01918	0.01343	0.00442	0.11321	0.11466	0.04299
H2	0.00165	0.00152	0.08891	0.01894	0.01374	0.00441	0.11985	0.12872	0.04722
H3	0.00166	0.00154	0.10499	0.01900	0.01324	0.00445	0.12771	0.14711	0.05246
H4	0.00165	0.00149	0.10721	0.01928	0.01314	0.00440	0.13364	0.16760	0.05605

 doi:10.20944/preprints202511.1691.v1

Based on the above results, the optimal mix proportion of AAFC was determined to be $A_3B_2C_1D_4E_4F_3G_1H_4$, with the following factor levels: alkali equivalent of 0.1, activator modulus of 1.1, water-to-binder ratio of 0.4, foam dosage of 4.5 (multiple of theoretical value), foam stabilizer dosage of 3.5% (by mass of foaming agent), aerogel dosage of 6 kg/m^3, calcium hydroxide dosage of 5% (by mass of FA), and waterproofing agent dosage of 5.5% (by mass of FA). The specimens were prepared and cured again according to the above mix proportion, and the performance parameters of the optimal mix AAFC were measured as follows: dry density of 576.34 kg/m^3, thermal conductivity of 0.1107 W/(m·K), mass water absorption rate of 3.87%, compressive strength of 5.83 MPa, flexural strength of 1.41 MPa, drying shrinkage of 0.614 mm/m, strength loss rate of 10.433%, and mass loss rate of 1.764%. This indicates that all the indicators of the AAFC with the optimal mix proportion meet the target requirements.

5. Conclusions

(1) A target performance system was established for ultralow energy buildings in hot-summer and cold-winter regions, comprising six primary and ten secondary indicators, with particular emphasis on water resistance.

(2) A volume-based mix design method was proposed for the AAFC. Preliminary mixes only met dry density targets, with mass water absorption reaching 57.1% (11.42 times the target), indicating the need for comprehensive optimization.

(3) An 8-factor, 4-level orthogonal experiment was designed. The SiO_2 aerogel (6 kg/m^3) effectively reduced the thermal conductivity without compromising its mechanical properties. The waterproofing agent (5.5% FA mass) achieved optimal water resistance and frost durability.

(4) The optimal mix proportion of AAFC was determined to be $A_3B_2C_1D_4E_4F_3G_1H_4$ by matrix analysis. The performance indicators were as follows: dry density 576.34 kg/m^3; thermal conductivity, 0.1107 W/(m·K); water absorption, 3.87%; compressive strength 5.83 MPa, flexural strength 1.41 MPa, drying shrinkage, 0.614 mm/m; frost resistance (10.433% strength loss and 1.764% mass loss). All parameters satisfied the target requirements.

Conflicts of Interest: The authors declare that they have no conflict of interest.

Acknowledgments: This research was supported by the Natural Science Foundation of the Jiangsu Higher Education Institutions of China(Grant No.22KJB560014), Jiangsu Collaborative Innovation Center for Building Energy Saving and Construct Technology Youth Doctoral Foundation (Grant No. SJXTBS2107).

References

1. China Association of Building Energy Efficiency, Chongqing University. Research Report on Carbon Emissions in China's Urban and Rural Construction Sector (2024 Edition) [R]. Beijing: China Association of Building Energy Efficiency, 2025.
2. Gencel, O., Yavuz Bayraktar, O., Kaplan, G., et al. Lightweight foam concrete containing expanded perlite and glass sand: Physico-mechanical, durability, and insulation properties. Construction and Building Materials, 320, 126187. DOI:10.1016/j.conbuildmat.2021.126187
3. Zhang W, Yu H, Yin B, et al. Effects of recycled carbon fibers on mechanical and piezoresistive properties and environmental impact in alkali-activated cementitious materials[J].Journal of Cleaner Production,2024,450141902-. DOI:10.1016/J.JCLEPRO.2024.141902
4. Hore S, Shiuly A. Study of thermal conductivity of different types of alkali-activated concrete:a comprehensive review[J] Environment Development and Sustainability,2023,27(3):1-48. DOI:10.1007/s10668-023-04118-8
5. Yılmazoğlu U M, Kara O H, Benli A, et al. Sustainable alkali-activated foam concrete with pumice aggregate: Effects of clinoptilolite zeolite and fly ash on strength, durability, and thermal performance[J].Construction and Building Materials, 2025,464140160-140160. DOI:10.1016/j.conbuildmat.2025.140160

 doi:10.20944/preprints202511.1691.v1

6. Bayraktar Y O, Özel B H, Benli A, et al. Sustainable foam concrete development: Enhancing durability and performance through pine cone powder and fly ash incorporation in alkali-activated geopolymers[J].Construction and Building Materials,2024,457139422-139422.DOI:10.1016/j.conbuildmat.2024.139422
7. Juntao D, Xiaosong T, Jianzhuang X, et al. Influence of alkaline activator and precursor on the foam characterization and alkali-activated foamed concrete properties[J]. Cement and Concrete Composites, 2024,145. DOI:10.1016/j.cemconcomp.2023.105341
8. Dang J, Tang X, Xiao J, et al. Role of recycled brick powder and alkaline solution on the properties of eco-friendly alkali-activated foam concrete[J].Journal of Cleaner Production,2024,436140381-. DOI:10.1016/j.jclepro.2023.140381
9. Benli A. Sustainable use of waste glass sand and waste glass powder in alkali-activated slag foam concretes: Physico-mechanical, thermal insulation and durability characteristics[J].Construction and Building Materials,2024, 438137128-137128. DOI:10.1016/j.conbuildmat.2024.137128
10. Xiong Y, Zhang Z, Huo B, et al. Uncovering the influence of red mud on foam stability and pore features in hybrid alkali-activated foamed concrete[J].Construction and Building Materials,2024,416135309-. DOI:10.1016/j.conbuildmat.2024.135309
11. Liu X, Jiang T, Li C, et al. Effect of Precursor Blending Ratio and Rotation Speed of Mechanically Activated Fly Ash on Properties of Geopolymer Foam Concrete[J].Buildings,2024,14(3): DOI:10.3390/buildings14030841
12. Chen L, Wang Z, Wang Y, et al. Preparation and properties of alkali activated metakaolin-based geopolymer[J].Materials,2016,9(9):767-767. DOI:10.3390/ma9090767
13. Wang S, Li H, Zou S, et al. Experimental research on a feasible rice husk/geopolymer foam building insulation material[J].Energy and Buildings, 2020,226(7):110358. DOI:10.1016/j.enbuild.2020.110358
14. Shakouri S, Bayer Z, Erdoan T S. Development of silica fume-based geopolymer foams[J].Construction and Building Materials,2020,260:120442. DOI:10.1016/j.conbuildmat.2020.120442
15. N. A B, M. E S, A. S S, et al. Improved Fly Ash Based Structural Foam Concrete with Polypropylene Fiber[J].Journal of Composites Science,2023,7(2):76-76. DOI: 10.3390/jcs7020076
16. Cui B L, Liu J, Li S, et al. Study on preparation and properties of cement-based/ geopolymer-polystyrene composite building exterior wall insulation materials[J]. Science of advanced materials, 2018, 10(11):1636-1645. DOI:10.1166/sam.2018.3384
17. Horvat B, Knez N, Hribar U, et al. Thermal insulation and flammability of composite waste polyurethane foam encapsulated in geopolymer for sustainable building envelope[J].Journal of Cleaner Production,2024,446141387-. DOI:10.1016/j.jclepro.2024.141387
18. Huiskes D, Keulen A, Yu Q, et al. Design and performance evaluation of ultra-lightweight geopolymer concrete[J].Materials Design,2016,89:516-526. DOI:10.1016/j.matdes.2015.09.167
19. Yifei H, Guangzhao Y, Kaikang L. Development of fly ash and slag based high-strength alkali-activated foam concrete[J].Cement and Concrete Composites,2022,104447-. DOI:10.1016/j.cemconcomp.2022.104447
20. Masi G, Tugnoli A, Bignozzi C M. Lightweight alkali activated composites by direct foaming based on ceramic tile waste and fly ash[J].Ceramics International,2024,50(24PC):55410-55420. DOI:10.1016/j.ceramint.2024.10.399
21. Siti A F, Liew M Y, Mohd A B A M, et al. Mechanical Properties and Thermal Conductivity of Lightweight Foamed Geopolymer Concretes[J].IOP Conference Series: Materials Science and Engineering,2019,551:012089-. DOI:10.1088/1757-899X/551/1/012089
22. Jaya A N, Yun-Ming L, Cheng-Yong H, et al. Correlation between pore structure, compressive strength and thermal conductivity of porous metakaolin geopolymer[J].Construction and Building Materials,2020,247:118641-. DOI:10.1016/j.conbuildmat.2020.118641.
23. SU L.J., FU G.S., LI F.Y., et al. Preparation and mechanical properties of coal gangue-based foamed geopolymer[J].Bulletin of the Chinese Ceramic Society, 2020, 39(11): 3549-3556. DOI:10.16552/j.cnki.issn1001-1625.2020.11.008

 doi:10.20944/preprints202511.1691.v1

24. Gao H, Liu H, Liao L, et al. A bifunctional hierarchical porous kaolinite geopolymer with good performance in thermal and sound insulation[J]. Construction and Building Materials, 2020, 251(9):118888-. DOI:10.1016/j.conbuildmat.2020.118888
25. BERKOUCHE A, BELKADI A A, NOUI A, et al. Modeling and optimization of eco-friendly cellular foam geopolymer with recycled concrete and glass wastes using Box-Behnken design[J].Structures,2025,76109054-109054. DOI: 10.1016/j.istruc.2025.109054
26. Xian R, Xiang Z, Jianxin Z, et al. Study on mechanical and thermal properties of alkali-excited fly ash aerogel foam concrete[J].Construction and Building Materials,2023,408. DOI:10.1016/j.conbuildmat.2023.133770
27. Pan P, Yang W, Guo Z. Improvement of thermal properties of foam concrete by incorporating silica aerogel particles[J].Construction and Building Materials,2025,478141450-141450. DOI:10.1016/j.conbuildmat.2025.141450
28. Yong cheng J, Qijun S. The Stabilizing Effect of Carboxymethyl Cellulose on Foamed Concrete[J].International Journal of Molecular Sciences,2022,23(24):15473-15473. DOI:10.3390/IJMS232415473
29. Ministry of Housing and Urban-Rural Development of the People's Republic of China. JGJ/T 341-2014 Technical specification for application of foamed concrete[S]. Beijing: China Architecture and Building Press, 2014.
30. Ministry of Housing and Urban-Rural Development of the People's Republic of China. JGJ/T 323-2014 Technical specification for application of self-insulation concrete compound block walls[S]. Beijing: China Architecture and Building Press, 2014.
31. Ministry of Housing and Urban-Rural Development of the People's Republic of China. GB 50574-2010 Technical specification for unified application of wall materials[S]. Beijing: China Architecture & Building Press, 2011.
32. Jiangsu Provincial Department of Housing and Urban-Rural Development. Technical guidelines for ultra-low energy residential buildings (trial implementation)[S]. Nanjing: Jiangsu Provincial Department of Housing and Urban-Rural Development, 2020.
33. Shanghai Municipal Housing and Urban-Rural Development Administration. Technical guidelines for ultra-low energy buildings (trial implementation)[S]. Shanghai: Shanghai Municipal Housing and Urban-Rural Development Administration, 2019.
34. Ministry of Housing and Urban-Rural Development of the People's Republic of China. GB/T 51350-2019 Technical standard for nearly zero energy buildings[S]. Beijing: China Architecture and Building Press, 2019.
35. Ministry of Housing and Urban-Rural Development of the People's Republic of China. GB 50176-2016 Code for thermal design of civil buildings[S]. Beijing: China Architecture and Building Press, 2017.
36. Ministry of Housing and Urban-Rural Development of the People's Republic of China. GB 50574-2010 Uniform technical code for wall materials used in buildings[S]. Beijing: China Architecture and Building Press, 2010.
37. China Building Materials Federation. JC/T 2199-2013 Foaming agent for foamed concrete[S]. Beijing: China Building Materials Industry Press, 2013.
38. Taohua Y, Jianzhuang X, Zhenhua D, et al. Geopolymers made of recycled brick and concrete powder-A critical review[J].Construction and Building Materials,2022,330. DOI:10.1016/j.conbuildmat..2022.127232
39. Mahmoud A A, Johnson U A, Sumiani Y, et al. Engineering performance of sustainable geopolymer foamed and non-foamed concretes[J].Construction and Building Materials,2022,316. DOI:10.1016/j.conbuildmat..2021.125601
40. Gu G, Xu F, Huang X, et al. Foamed geopolymer: The relationship between rheological properties of geopolymer paste and pore-formation mechanism[J].Journal of Cleaner Production,2020,277. DOI:10.1016/j.jclepro.2020.123238
41. Ryu S G, Lee B Y, Koh T K, et al. The mechanical properties of fly ash-based geopolymer concrete with alkaline activators[J].Construction and Building Materials, 2013,47409-418. DOI:10.1016/j.conbuildmat.2013.05.069

 doi:10.20944/preprints202511.1691.v1

42. Burak B, Yavuz O B, Ahmet B, et al. Effect of using wastewater from the ready-mixed concrete plant on the performance of one-part alkali-activated GBFS/FA composites: Fresh, mechanical and durability properties[J].Journal of Building Engineering,2023,76. DOI:10.1016/J.JOBE.2023.107167
43. K. S J, Yashida N, K. G. Effect of source materials, additives on the mechanical properties and durability of fly ash and fly ash-slag geopolymer mortar: A review[J].Construction and Building Materials,2021,280. DOI:10.1016/j.conbuildmat.2021.122443
44. D. C W, Ranjani S I G. Investigations on the performance of xanthan gum as a foam stabilizer and assessment of economic and environmental impacts of foam concrete production[J].Journal of Building Engineering,2024,82108286-. DOI:10.1016/J.JOBE.2023.108286
45. Oguzhan B Y, Gokhan K, Osman G, et al. Physico-mechanical, durability and thermal properties of basalt fiber reinforced foamed concrete containing waste marble powder and slag[J].Construction and Building Materials,2021,288. DOI:10.1016/j.conbuildmat.2021.123128
46. Chao-Lung H, Damtie M Y, Duy-Hai V, et al. Performance evaluation of alkali activated mortar containing high volume of waste brick powder blended with ground granulated blast furnace slag cured at ambient temperature[J].Construction and Building Materials,2019,223657-667. DOI:10.1016/j.conbuildmat.2019.07.062
47. Youjie S, Yunchuan P ,Shanwen Z, et al. Thermal stability of foams stabilized by fluorocarbon and hydrocarbon surfactants in presence of nanoparticles with different specific surface areas[J].Journal of Molecular Liquids,2022,365. DOI:10.1016/J.MOLLIQ.2022.120187
48. Liu X, Wu Y, Li M, et al. Effects of graphene oxide on microstructure and mechanical properties of graphene oxide-geopolymer composites[J]. Construction and Building Materials,2020,247118544-118544. DOI:10.1016/j.conbuildmat.2020.118544
49. Lijuan S, Guosheng F, Bing L, et al. Working performance and microscopic mechanistic analyses of municipal solid waste incineration (MSWI) fly ash-based self-foaming filling materials[J]. Construction and Building Materials,2022,361. DOI:10.1016/j.conbuildmat.2022.129647
50. Pasupathy K, Ramakrishnan S, Sanjayan J. Enhancing the mechanical and thermal properties of aerated geopolymer concrete using porous lightweight aggregates[J].Construction and Building Materials,2020,264. DOI:10.1016/j.conbuildmat.2020.120713
51. Yu P, Kirkpatrick R J, Poe B, et al. Structure of calcium silicate hydrate (C-S-H): Near-, Mid-, and far-infrared spectroscopy[J].Journal of the American Ceramic Society, 2010, 82(3):742-748. DOI:10.1111/j.1151-2916.1999.tb01826.x